ARTICLES
https://doi.org/10.1038/s41550-022-01755-3
nature astronomy

Check for updates

OPEN

Detection of an excess of young stars in the Galactic Centre Sagittarius B1 region

Francisco Nogueras-Lara[1]✉, Rainer Schödel[2] and Nadine Neumayer[1]

The Milky Way's centre is the closest galaxy nucleus and the most extreme environment in the Galaxy. Although its volume is less than 1% of that of the Galactic Disk, up to 10% of all new stars in the Galaxy in the past 100 Myr formed there. It therefore constitutes a perfect laboratory to understand star formation under extreme conditions, similar to those in starburst or high-redshift galaxies. However, the only two known young clusters in the Galactic Centre account for <10% of the expected young stellar mass. We analyse the star formation history of Sagittarius (Sgr) B1, a Galactic Centre region associated with strong H II emission, and find evidence for the presence of several 10^5 solar masses of young stars that formed ~10 Myr ago. We also detect the presence of intermediate-age (2–7 Gyr old) stars in Sgr B1 that seem to be rare (or absent) in the inner regions of the nuclear stellar disk, and might indicate inside-out formation. Our results constitute a large step towards a better understanding of star formation at the Galactic Centre, such as the fate of young clusters, and the possibly different initial mass function in this region.

The Milky Way's centre is located at only 8 kpc from Earth and constitutes the only galaxy nucleus where we can resolve individual stars down to milliparsec scales[1,2]. It is roughly delimited by the central molecular zone and the nuclear stellar disk (a dense, stellar disk-like structure)[3,4]. The nuclear stellar disk is characterized by high stellar densities, strong tidal fields, high magnetic fields and both high levels of turbulence and high temperatures in the interstellar medium[3,5,6]. In spite of—or possibly because of—these harsh conditions, the Galactic Centre emits more than 10% of the total Galactic Lyman continuum flux despite occupying less than 1% of the total Galaxy volume[7]. Studies of the radio to high-energy emission, the finding of massive young stars throughout its region, the detection of classical Cepheids and the star formation history (SFH) inferred from luminosity functions all indicate that star formation reached rates on the order of 0.1 solar mass ($M_\odot$) per year in the Galactic Centre in the past 10–100 Myr (refs. [4,8–11]). Therefore, it constitutes a unique laboratory to study star formation under extreme conditions. However, there are only two young massive clusters known (Arches and Quintuplet), which account for less than 10% of the total young stellar mass expected[12]. This is the so-called missing clusters problem. A plausible explanation for this is the rapid dissolution of even the most-massive clusters due to the tidal field in the Galactic Centre and encounters between the young clusters and massive molecular clouds[13,14]. Moreover, the high stellar background density[2] combined with the strong and patchy interstellar extinction towards the Galactic Centre[15] hamper the detection of all but the tightest and most-massive young clusters, as well as the detection of individual young stars, and restrict their analysis to mainly the near-infrared regime. The creation of a complete census of recent star formation in this region is therefore a formidable challenge.

Sagittarius (Sgr) B1 is a well-known region associated with strong H II emission in the nuclear stellar disk[16]. Far-infrared observations suggest the presence of widely spaced hot stars that excite the gas in at least eight separate subregions[16,17]. Moreover, a cohort of six young massive stars (O-type and WN7-9ha) have been detected there[11,18]. In this work, we use the GALACTICNUCLEUS survey[1,2]—a high-angular-resolution (~0.2″) JHK$_s$-band catalogue specifically designed to observe the Galactic Centre—to study a field of ~160 pc^2 covering part of the Sgr B1 region (centred on 17 h 47 m 15.41 s, 28° 31′ 39.7″, Fig. 1) and compare it with a control field of similar size in the inner nuclear stellar disk region (centred on 17 h 45 m 20.81 s, 28° 57′ 58.6″, Fig. 1). We chose this control field because it was observed under similar excellent conditions to the target field[2] (seeing in the H and K$_s$ bands is ~0.4″), and because it does not contain any obvious structures, such as the Arches or Quintuplet clusters, or the nuclear star cluster.

Given the significantly different extinction along the line of sight between the Galactic Centre and the Galactic Disk, we applied a colour cut in the $H-K_s$ colour–magnitude diagram to remove foreground stars[4,19] (Fig. 2). We then built extinction maps using red giant stars (whose intrinsic colour, $(H-K_s)_0$, is approximately constant) to correct for reddening and differential extinction[15]. Finally, we created a K$_s$ luminosity function (KLF, Fig. 3, corrected for completeness), which provides the number of stars per luminosity interval.

The KLF of a stellar population contains information about its formation history[4,20]. We fitted the KLFs of Sgr B1 and the control field with a linear combination of theoretical models applying Monte Carlo simulations (Methods). The KLF of a single-age population changes as a function of age, with the variability timescales shortening towards younger ages. We chose particularly closely spaced samples for the youngest ages (5–40 Myr ago (Ma)). We used two different sets of stellar evolutionary models that properly cover the youngest stellar populations to deal with possible systematics (PARSEC[21–23] and MIST[24–26]). We assumed a metallicity of twice solar in agreement with recent results for the Galactic Centre[4,27,28].

Results

Figure 4a,b shows the obtained SFH for Sgr B1 and the control field. We also applied the same technique to a KLF of the central region of the nuclear stellar disk directly taken from a previous study[4] (~1,600 pc^2, indicated in Fig. 1) to compare the SFHs (Fig. 4c). For this comparison, we excluded the nuclear star cluster as it exhibits a

[1]Max-Planck Institute for Astronomy, Heidelberg, Germany. [2]Instituto de Astrofísica de Andalucía (CSIC), Granada, Spain. ✉e-mail: nogueras@mpia.de

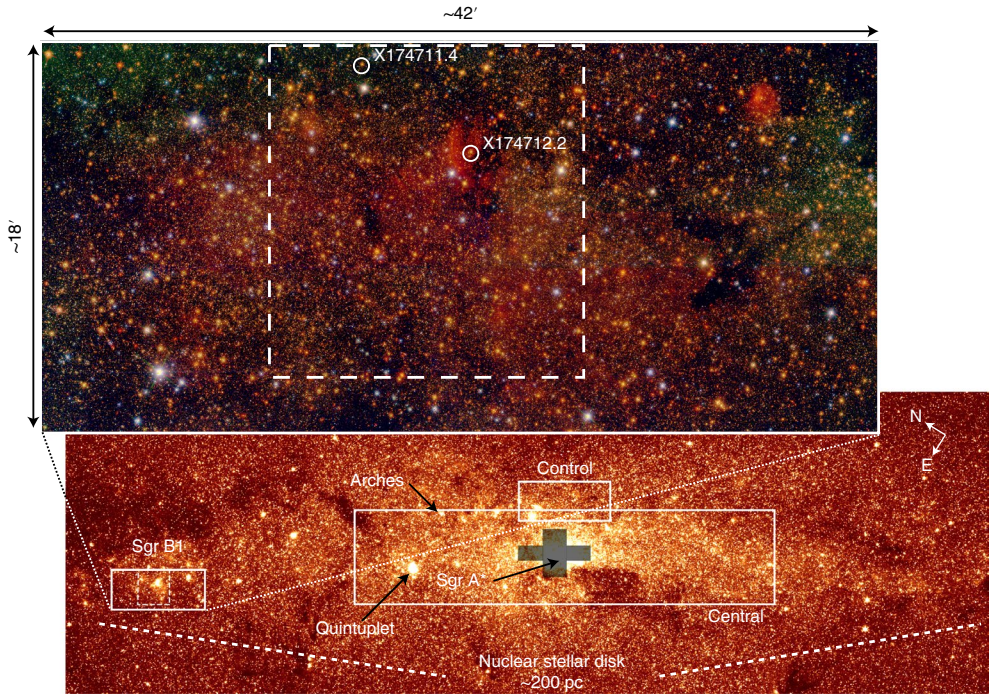

Fig. 1 | Scheme of the analysed regions. The regions studied (the Sgr B1, control and central nuclear disk fields) are plotted over a Spitzer 4.5 μm image[34]. The black shaded cross indicates a region of low completeness dominated by the nuclear star cluster that was excluded from the analysis of the central field[4]. The positions of the Arches and Quintuplet clusters and Sgr A* are indicated. The close-up of the region indicated by the left white box is a JHK_s GALACTICNUCLEUS false-colour image, with dimensions of 8 pc and 18.5 pc. The dashed rectangle indicates the region of intense hot dust emission that was specifically studied. Two Wolf–Rayet stars[11] within the analysed region are indicated by white circles.

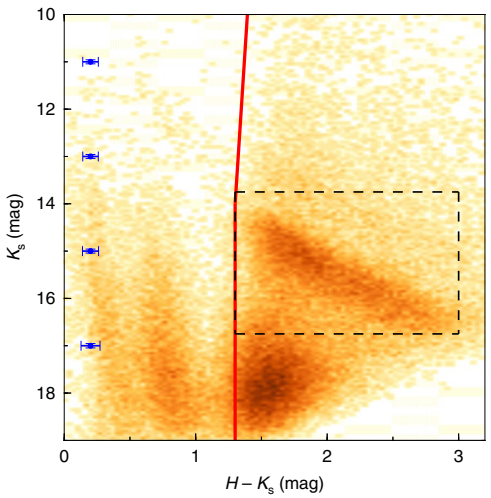

Fig. 2 | $H - K_s$ colour–magnitude diagram for the Sgr B1 field. The red line shows the colour cut made to remove foreground stars. The black dashed rectangle indicates the red giant stars used to compute the extinction map. The blue error bars show the 1σ mean uncertainties of the data. Vega H and K_s magnitudes are used in the figure.

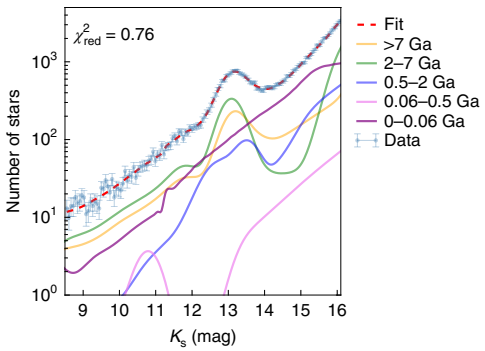

Fig. 3 | Analysis of the Sgr B1 KLF. The Sgr B1 KLF (blue data points) was corrected for extinction, completeness and saturation. The error bars show the 1σ uncertainties per brightness bin. The red dashed line indicates the best-fit model (of the PARSEC models) whose reduced χ^2 is indicated in the figure. Coloured lines depict the contributions of the different age bins.

significantly different SFH[4,20,29] and might thus bias the results. The results for the control and the inner Galactic Centre fields agree with previous work for the central region of the nuclear stellar disk[4]: the bulk of stars ($\gtrsim$80% of the stellar mass) in both fields are older than 7 Ga. There was a distinct epoch of star formation between 0.5 and 2 Ga, in which we found a significant contribution from the stellar models with ages of ~1 Ga, corresponding to the massive star forming event that took place ~1 Ga in the nuclear stellar disk[4]. Star formation continued at lower rate until the present day. On the other hand, the SFH of the Sgr B1 region is significantly different. The stellar population is younger on average, and there is an important contribution from an intermediate-age (2–7 Ga) population (~40% of the total stellar mass), suggesting a more continuous SFH than in the innermost regions of the Galactic Centre. Moreover, the star formation activity between 0.5 and 2 Ga is more prominent. Finally, we detected a much larger contribution from young stars in comparison to the control field. In particular, the youngest age bin (<60 Ma) accounts for more than 5% of the total stellar mass of the Sgr B1 region, six times more than in the control field.

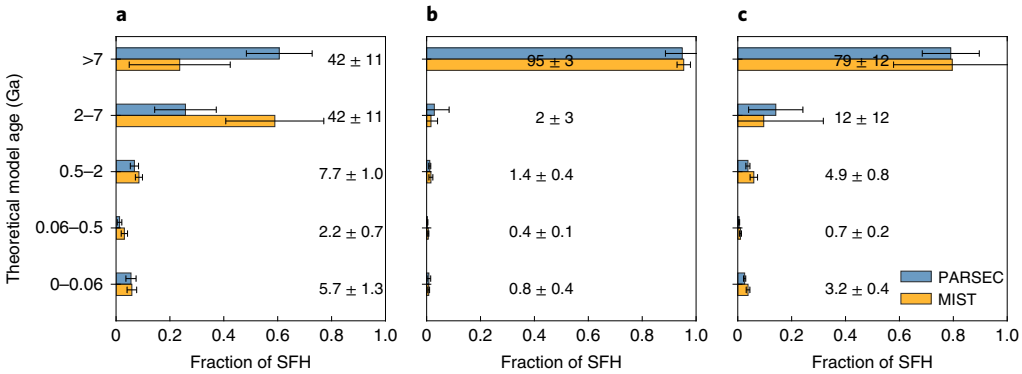

Fig. 4 | SFHs of the analysed regions. a–c, SFHs of the Sgr B1 region (**a**), the control region (**b**) and the central region of the nuclear stellar disk (**c**). The error bars show the 1σ uncertainties. The numbers in each panel indicate the percentage of the total stellar mass per age interval computed as an average between PARSEC and MIST models (see 'Model fitting and SFH calculations' in the Methods).

This contribution from young stars is also around two times higher than in the central region of the nuclear disk, where we detected a higher fraction of young stars than in the control field due to the presence of the Arches and Quintuplet clusters, as well as probably unknown stellar associations in this large field[30].

On the other hand, the presence of a significantly different contribution from the intermediate-age stellar population in the Sgr B1 region, compared with the control and the inner Galactic Centre fields, may be indicative of inside-out formation of the nuclear stellar disk. Such an age gradient has also been observed in external galaxy nuclei and used to propose the inside-out formation channel of nuclear stellar disks[31].

Using PARSEC models, we estimated that the Sgr B1 field studied here contains a total originally created stellar mass of $7.6 \pm 0.7 \times 10^6\,M_\odot$. This implies that the youngest stellar population accounts for $4.3 \pm 1.1 \times 10^5\,M_\odot$, nearly an order of magnitude higher than the combined mass of the Arches and Quintuplet clusters[32,33]. We investigated the presence of young stars in Sgr B1 further by carrying out a dedicated analysis of a small region (~40 pc^2, white dashed rectangle in Fig. 1) that contains intense dust emission in the Spitzer image[34] (4.5 μm), probably caused by young hot stars. We found that more than 7% of the total stellar mass is due to young stars (<60 Ma). We also estimated the age of the stars in this region by analysing the contribution of the considered young stellar models (5, 10, 20 and 40 Ma) to each of the Monte Carlo samples (Methods). Using PARSEC and MIST models, we found that the 5 + 10 Ma model populations significantly contributed to ~99% of all Monte Carlo samples, and correspond to 6 ± 1% of the total stellar mass (Fig. 5), accounting for almost the full mass of young stars (0–60 Ma) in the region. Therefore, we estimated that this region contains $\sim 1.2 \times 10^5\,M_\odot$ of stars with ages between 5 and 10 Ma. A similar analysis carried out for the whole Sgr B1 field indicated that 2 ± 2% of the total stellar mass is due to young stars with ages between 5 and 10 Ma. We thus concluded that the ~40 pc^2 region with intense hot dust emission presents an overabundance of young stars of these ages in comparison with the surrounding area.

The Sgr B1 region is located at a radial distance of ~80 pc from the supermassive black hole Sgr A*. This implies a rotation period of ~5 Myr for its stellar population, assuming a circular velocity of ~100 km s^{-1} (ref. [35]). Our age estimate for the detected young stellar population thus suggests that it was not formed in situ and has already orbited the nuclear stellar disk at least once. This agrees with previous work proposing that the exciting sources of Sgr B1 did not originate there[16,17,36]. Hence, the detected H II emission is a consequence of the ionization of the envelope of molecular gas and dust found in the Sgr B complex by stars widely spread throughout the field[16]. This scenario also explains the detection of some young stellar objects in the Sgr B1 region as a very recent star formation event (different from the detected young stellar population), triggered by outflows from the ionizing stars[16].

On the other hand, the presence of a cohort of six O-type and WN7-9ha X-rays emitter stars in this region with apparent coeval evolution and in relative proximity suggests that they constitute a distinct physically related group[18]. A comparison of this stellar population with the Arches cluster, of which only four members are known X-ray emitters[37], suggests that the Sgr B1 cohort of known hot massive stars could be representative of a similarly rich massive stellar population[18] in good agreement with our findings. In addition, the presence of a supernova remnant candidate in the Sgr B1 region[38], near the detected young stellar association (~15 pc away from it), provides further evidence for the presence of a young stellar population, in agreement with our results.

Determining the location where the detected young stellar population formed is very challenging due to its age uncertainty and the unknown distance along the line of sight, which impede an accurate orbit reconstruction. Given the estimated high mass of the young stellar population ($\sim 10^5\,M_\odot$), it seems unlikely that the young stars were formed as a single bound cluster. Moreover, theoretical studies point towards an upper limit of $\sim 10^4\,M_\odot$ for the formation of bound clusters in the central molecular zone[39]. Therefore, we conclude that the detected young stellar population probably formed as a coeval stellar association. Nevertheless, extrapolating the cluster formation efficiency observed in the close Galactic Centre cloud Sgr B2 (where ~40% of the stars are forming in gravitationally bound clusters[40]), it is likely that some of the young stars in Sgr B1 could have constituted several gravitationally bound clusters. This can be used to estimate a lower limit on the age of the detected stellar population, given that there is no clear stellar overdensity in the Sgr B1 region, pointing towards a rapid dispersion of the possible young clusters below the high stellar background density in the Galactic Centre. In this way, the age that we estimate for the detected young stellar association is consistent with the predicted short disruption time of gravitationally bound clusters (~6 Myr), caused by tidal shocking by giant molecular clouds in the central molecular zone[14]. Moreover, it also agrees with the previously inferred recent SFH in the Galactic Centre that presents a maximum in star formation around 10 Ma (ref. [41]).

Our findings constitute the detection of a significant mass of recently formed stars at the Galactic Centre beyond the Arches and Quintuplet clusters and the known isolated massive stars. Our results may indicate the fate of the Arches and Quintuplet clusters, which are around 5 Myr younger than the detected young stellar population.

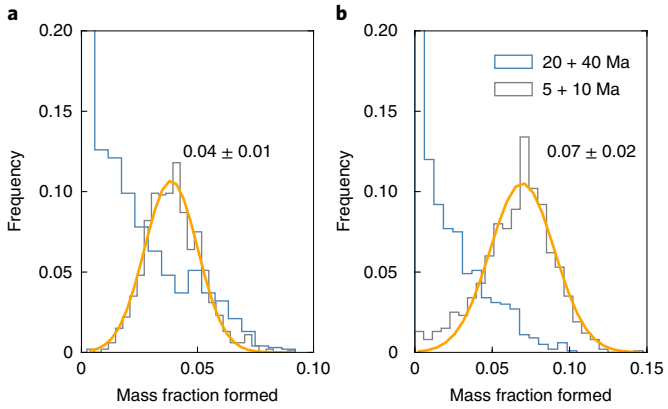

Fig. 5 | The contribution of young populations to the KLF of the Sgr B1 hot dust emission region. a, Results from PARSEC models. **b**, Results from MIST models. The yellow lines show a Gaussian fit to the distribution of 5 + 10 Ma. The mean and the standard deviation (1σ uncertainty) are indicated in each panel.

In this way, they contribute to a more general picture of the evolution of the young stars in the Galactic Centre in which stars form in massive stellar associations that can contain clusters (Sgr B2 is an example of this stage[40]) and later disperse while orbiting through the nuclear stellar disk. Our findings also help us to understand the isolated massive stars detected across the Galactic Centre, whose proper motions indicate that they are not related to the known young clusters[42], supporting their formation in stellar associations or gravitationally bound clusters that dispersed on relatively short timescales after their formation several million years ago.

Methods

Data. For this work, we used H and K_s data from the GALACTICNUCLEUS survey[1,2], which is publicly available on the ESO Phase 3 data release archive. This is a high-angular-resolution (~0.2″) JHK$_s$ survey of the Galactic Centre especially designed to observe its stellar population and overcome the extreme extinction and source crowding. It contains accurate photometry of ~3.3×10^6 stars covering a total area of ~6,000 pc^2. The photometric statistical uncertainties are below 0.05 mag at $H\approx19$ mag and $K_s\approx18$ mag. The zero-point systematic uncertainty is $\lesssim$0.04 mag in all bands. In particular, we used two individual pointings (D12 and F19)[2] that partially cover the Sgr B1 region and a control field and were observed under similar excellent conditions (seeing in the H and K_s bands is ~0.4″). As comparing fields, we also used data from pointing F10, containing the Quintuplet cluster, and the 14 central pointings of the survey that cover the central region of the nuclear stellar disk[4]. For the latter case, we directly used the final KLF as it was obtained in previous work[4], where the nuclear star cluster—which constitutes a distinct component with different origin, SFH and stellar population than the nuclear stellar disc—was removed to avoid biasing the results. The observing conditions of these 14 fields were worse than those for the target and control fields (seeing in the H and K_s bands is ~0.6″), and thus the faint end of the KLF is ~1 mag lower. Moreover, the central region of the GALACTICNUCLEUS survey has low completeness for its innermost field (the cross-shaped region in Fig. 1), impeding a proper analysis of the KLF of the nuclear star cluster to derive its SFH.

Before our analysis, we corrected potential saturation problems in K_s for stars brighter than 11.5 mag (ref. [2]). To do this, we used the SIRIUS IRSF[43] survey of the Galactic Centre to replace the photometry of saturated stars and also completed the list with bright stars that might have escaped detection in the GALACTICNUCLEUS catalogue.

Extinction maps. For each of the analysed regions, we created a dedicated extinction map using red clump stars[44] (red giant stars in their helium burning phase), which are very abundant and homogeneously distributed across the field and have a well-defined intrinsic colour[15] $(H-K_s)_0=0.10\pm0.01$ mag. We also included red giant stars (with very similar intrinsic colours $H-K_s$)[4,15] to increase the angular resolution of the maps. To choose the reference stars, we used a colour cut in the colour–magnitude diagrams as shown in Fig. 2 (black dashed rectangle). We built the extinction maps following the methodology described in our previous work[15] and assumed an extinction curve[45] $A_H/A_{Ks}=1.84\pm0.03$, where A_H and A_{Ks} indicate the extinction in H and Ks. We defined a pixel size of ~2″ and computed the associated extinction values for each pixel by using the five closest reference stars in a maximum radius of 7.5″. We weighted the distances using an inverse-distance weight method and assumed a maximum colour difference of 0.3 mag between the stars to avoid mixing stars with extinctions that were too different. If fewer than five reference stars were detected for a given pixel, we did not assign any extinction value. Supplementary Fig. 1 shows the extinction maps obtained for the Sgr B1 and control fields (F19). Using a jackknife resampling method, systematically leaving out one of the reference stars for each pixel, we obtained a statistical uncertainty for the extinction maps of ~3%. The systematics were estimated by quadratically propagating the uncertainties of the quantities involved in the extinction calculation. We obtained a mean systematic uncertainty of ~5%.

Dereddening. Given the extreme differential extinction along the observed line of sight, it is possible to remove the foreground stellar population—belonging to the Galactic Disk and Bulge—by applying a colour cut off H–$K_s\approx1.3$ mag (ref. [19]) (red solid line in Fig. 2). We then applied the previously computed extinction maps to deredden each of the studied fields. Supplementary Fig. 2 shows the colour–magnitude diagrams of $H-K_s$ for the Sgr B1 field and the control region before and after applying the extinction maps. To check that the differential extinction was significantly corrected, we computed the standard deviation of the distribution of red clump stars before and after the extinction correction and found that the scatter of red clump stars is approximately eight times lower in the corrected sample.

KLFs. To create the KLFs, we used all the K_s dereddened stars (including stars that were not detected in the H band)[4], after excluding the foreground population. We also removed over-dereddened stars by excluding stars with a dereddened $H-K_s$ colour 2σ bluer than the one from the mean distribution of the dereddened red clump feature. Around 3% of the stars were removed by applying this technique for the analysed Sgr B1 region. They corresponded to stars with an average $H-K_s\approx1.6$ mag that is considerably lower than the mean value of the whole stellar population ($H-K_s\approx2$ mag). We concluded that they are likely to be foreground stars from the Galactic Bulge that passed the previous colour cut but are not still behind the full extinction screen for the Galactic Centre.

We created the KLFs using a bin width that maximized the Freedman–Diaconis[46] and Sturges[47] estimators. We computed the uncertainties considering Poisson errors (that is, the square root of the number of stars per bin).

Completeness. We also corrected for completeness by computing a solution based on artificial stars tests. Namely, we created 20 modified science images for each field inserting ~5% of the total number of stars in magnitude bins of 0.5 mag starting from $K_s=12$ mag. We then used the StarFinder software[48] to measure point-spread-function photometry following the same procedure used to create the GALACTICNUCLEUS survey[1,2] and checked the fraction of recovered artificial stars to estimate the completeness correction. Supplementary Fig. 3 indicates the completeness solution for the Sgr B1 and the control fields. The uncertainties were estimated via the standard deviation of the completeness solution of the results obtained for each of the four independent HAWK-I chips that constitute each field[1]. We found that the completeness was higher for the Sgr B1 region, which can be explained by the higher stellar crowding in the control field that is closer to the innermost regions of the Galactic Centre.

We computed an extinction correction for each completeness solution by calculating the median extinction of the stars constituting each KLF. We then completed the KLFs setting a lower limit of 75% of data completeness. We estimated the uncertainty per magnitude bin by quadratically propagating the uncertainties from the completeness solution and the original KLF[4].

Saturation. We restricted the analysis of the dereddened KLF to $K_s>8.5$ mag to avoid problems due to the potential saturation of bright stars in the SIRIUS IRSF catalogues[49]. We tested this saturation limit using 2MASS data[50], the lower angular resolution (~2″) of which makes it ideal to observe bright stars without saturation. We used 2MASS H and K_s photometry in the Sgr B1 region defined in this work and searched for common stars to establish a common photometric zero point. We then removed foreground stars in the 2MASS data by using a colour cut around $H-K_s\approx1.3$ mag, as previously explained. We applied the extinction map derived for the Sgr B1 region and created a K_s luminosity function corrected for extinction. Supplementary Fig. 4 shows the comparison between the 2MASS and the KLFs used. We conclude that, given the saturated sources in our sample that are potentially not detected, the KLF is significantly incomplete for $K_s<8.5$ mag.

Model fitting and SFH calculation. The KLF contains fundamental information about the SFH that can be reconstructed by studying its shape and the properties of its main features[4,20,29]. In this way, stellar populations with different ages present characteristic KLFs, as is shown in the 'Theoretical models' section. The main features[51] observed in the KLFs are the asymptotic giant branch bump (due to stars at the beginning of He shell-burning asymptotic giant branch evolution), the red clump bump (caused by red giant stars burning He in their cores), the red giant branch bump (due to old stars whose H-burning shell approaches the composition discontinuity left by the deepest penetration of the convective envelope during the

first dredge-up[52]) or the ascending giant branch (which contains stars evolving after the main sequence). Moreover, the presence of young stars ($\lesssim$10 Ma) can be identified due to an increased number of counts fainter than the red clump, in contrast to older populations (see the 'Theoretical models' section) that appear as a consequence of bright main sequence stars. In this way, we checked that the KLFs from the Sgr B1 and the control regions were significantly different (Supplementary Fig. 5), which would point towards the presence of different stellar populations (and probably young stars, $\lesssim$10 Ma), as we later confirmed with a careful analysis of the KLF.

We derived the SFH of each of the studied regions by fitting the KLFs with a linear combination of theoretical models[4,20]. To search for young stars that are potential tracers of dissolved clusters, we used PARSEC models[21–23] as a reference, given that they properly cover young stellar ages. We chose 14 individual ages for the model fit that homogeneously sample the possible ages of the analysed stellar populations: 14, 11, 8, 6, 3, 1.5, 0.6, 0.4, 0.2, 0.1, 0.04, 0.02, 0.01 and 0.005 Ga. We assumed a Kroupa initial mass function (IMF) corrected for unresolved binaries[53], and a stellar metallicity of around twice solar ($Z=0.03$), in agreement with previous results for the Galactic Centre[4,27,28]. To fit the KLFs, we included a parameter to account for the distance modulus (~14.6 at the distance of the Galactic Centre) and allowed it to vary within 3σ of the quadratically propagated uncertainties of the distance and the uncertainty of the dereddening process. We also included a Gaussian smoothing parameter to account for possible distance and/or differential extinction variations of the considered stellar populations.

To compute the SFH of each region, we resorted to Monte Carlo simulations, creating 1,000 KLFs obtained by randomly varying the number of stars per bin assuming the 1σ uncertainty as the standard deviation of the distribution. We then fitted each of the Monte Carlo samples using a χ^2 minimization criterion and obtained the SFH as the average of the results. To minimize possible degeneracies between models with similar ages, we combined them into five final age bins, as shown in Fig. 4a–c. The 1σ uncertainty was obtained via the standard deviation of the results in each age bin. To address potential systematic effects due to model selection, we repeated the procedure assuming MIST models[24–26] that were independently created and also adequate to trace the young stellar ages. We chose similar ages, a metallicity of around twice solar and a Salpeter IMF. The final value for each of the five age bins was computed by averaging over the results obtained with PARSEC and MIST models. We estimated the final uncertainties by quadratically propagating the ones independently obtained using PARSEC and MIST models.

We fitted the KLFs computed for the Sgr B1 and control regions, and also the KLF derived for the central region of the nuclear stellar disk in our previous work[4] (where the final uncertainties were larger owing to the lower completeness of the KLF due to the poorer data quality). We found a significantly different SFH in the Sgr B1 region, where there is a decrease of the contribution of old stars compensated by an increase of intermediate-age stars, and a significant contribution of young stars, suggesting the presence of an association of young stars.

We analysed potential sources of systematic uncertainties to assess the obtained results.

Stellar metallicity. We used PARSEC models assuming solar and 1.5 solar metallicities to assess the results in the Sgr B1 region. The results agree within the uncertainties with the obtained for twice solar metallicity using PARSEC models. The only difference is a higher contribution of the youngest stellar population for lower metallicities (~7% and ~8% for 1.5 solar and solar metallicity, respectively).

KLF bin width. We analysed the possible influence of the bin width on the derived SFH by repeating the process for new KLFs for the Sgr B1 and the control field, assuming half and double the previously computed bin width (0.03 and 0.12 mag for the Sgr B1 region, and 0.06 and 0.22 mag for the control field). The results are consistent with those obtained using PARSEC models and the original bin width. To further assess whether the data binning influenced our results, we used cumulative luminosity functions, which allowed us to eliminate the binning as a possible source of systematics. We built a cumulative KLF for the Sgr B1 region and fitted it with PARSEC theoretical models applying our Monte Carlo simulation approach. Given the saturation of the data for dereddened stars below $K_s=8.5$ mag, we assumed the distance-modulus solution obtained for the standard KLF method previously explained and computed the theoretical cumulative models without considering stars brighter than $K_s=8.5$ mag that are not present in the real data and would significantly bias the results. This is one of the main disadvantages of this method and implies that a priori parameters must be assumed for a proper fit. Moreover, cutting the bright end of the models requires us to restrict the fit to a minimum value of $K_s=8.75$ mag to avoid a starting point of the models at the same magnitude as the real data. We assumed the ages and metallicity previously specified for PARSEC models. We applied this technique to the Sgr B1 field and obtained results that were compatible with the ones obtained by using the standard KLF fitting method, as shown in Supplementary Fig. 6.

Faint end of the KLF. Given the different completeness of the Sgr B1 and the control fields (see the 'KLF' section), we studied the influence of the deeper Sgr B1 photometry on the results. In this way, we repeated the analysis restricting the Sgr B1 KLF to the faint-end limit of the KLF of the control region (15.36 mag). We did not observe any significant difference within the uncertainties.

Bright end of the KLF. We restricted the study of the KLFs to a $K_s>8.5$ mag limit to avoid any saturation problems related to the SIRIUS IRSF survey. Nevertheless, we also repeated the analysis of the Sgr B1 KLF with a less conservative limit of $K_s>7.5$ mag. We concluded that there is no significant variation on the results within the uncertainties.

Completeness solution. We based our completeness corrections on artificial star tests. To assess our completeness solution, we also estimated the completeness using an alternative approach based on the determination of the critical distance at which a star of a given magnitude can be detected around a brighter star[54]. This method is less accurate and constitutes a rough completeness estimation that mainly accounts for the completeness due to crowding. We obtained that the completeness is ~5–10% lower than that found using the artificial stars test. We checked whether this different completeness solution influenced our results, repeating the Sgr B1 KLF analysis by assuming the new completeness solution. We did not observe any variation within the uncertainties.

Different IMFs. There is some evidence of a top-heavy IMF for the known young clusters at the Galactic Centre[32]. We therefore repeated the analysis of the Sgr B1 KLF considering an IMF with $\alpha=1.8$ using MIST models and twice solar metallicity. We found that the SFH significantly changed for old ages: the contribution from stellar models >7 Ga shifted towards the 0.5–2 Ga age bin. Nevertheless, the results for the youngest stellar bin did not change within the uncertainties, leaving the conclusion about the young stars unaffected. We believe that the age shift for the oldest stellar population is due to the need to account for a stellar population enhanced in alpha elements[55] when a top-heavy IMF is assumed, that was not considered due to the limitations of current models. Moreover, this alpha enhancement is required only for the young stars and might not be representative of the bulk of stars, making it probably necessary to use different metallicities and enhancement in alpha elements for stellar populations with different ages. On the other hand, the mean χ^2 computed for the described top-heavy models is significantly higher than for the standard case of using twice solar metallicity without an enhancement in alpha elements. In any case, we conclude that the results for the youngest stellar population are robust.

Unresolved multiple stellar systems. We expected that a significant number of unresolved multiple stellar systems would affect the KLF given the results obtained for local stellar populations[56]. To check the impact of stellar multiplicity in our results, we used the SPISEA python package[57] to compute theoretical luminosity functions accounting for unresolved multiple systems. We defined the multiplicity fraction, the companion star frequency and the mass ratio between the multiple systems components using the standard SPISEA parameters based on observations of young clusters[58] (<10 Myr), which correspond to the young stellar population that we find in our analysis. We computed theoretical KLFs using MIST models[24–26] (implemented in the SPISEA package) assuming around twice solar metallicity and a slightly different age range due to the limitation of the models in SPISEA. In this way, we used 13 theoretical models with the following ages: 10, 8, 6, 3, 1.5, 1, 0.4, 0.2, 0.1, 0.04, 0.02, 0.01 and 0.005 Ga. We applied our method to fit the KLFs corresponding to the Sgr B1 region and the control field. We restricted the bright end of the KLFs to $K_s=9$ mag due to the limitations of the models. The results are consistent with our findings for both the Sgr B1 and control regions.

Theoretical models. We used PARSEC models[21–23] (version 1.2S+COLIBRI S37) as a main tool to derive the SFHs of the analysed regions. These models are designed to build synthetic stellar populations, assuming a solar-scaled metal mixture. PARSEC includes pre-main sequence stars to the thermally pulsing asymptotic giant branch and considers a wide range of metallicities and ages. We sampled the age range to cover the main features visible in the KLFs in the analysed magnitude range. In particular, the KLFs changed slowly for old stellar populations (>7 Ga), but more rapidly for younger ages (<2 Ga), at which we increased the number of stellar models considered. In this way, we were able to reconstruct the SFH of a given stellar population by assuming a linear combination of the chosen theoretical models. Supplementary Fig. 7 shows the 14 theoretical models used.

To assess the results and analyse possible sources of systematic uncertainties due to the construction of the models, we repeated our analysis using MIST models[24–26]. They constitute a fully independent set of self-consistent models with solar-scaled abundance ratios and extend across all evolutionary phases for all relevant stellar masses. We used a slightly different age range to properly cover the variation of the main features of the KLFs, sampling the whole age–space parameter range. This allowed us to cover the change in brightness for red clump stars around ~1 Ga (refs. [4,44]) that appears for slightly different ages between PARSEC and MIST models (1.5 and 1 Ga, respectively).

Given the smooth transition between models with similar ages, some degeneracy is expected. To decrease this potential degeneracy, we defined five larger age bins that included stellar populations with similar ages and considered the ages defined for both PARSEC and MIST models.

Youngest stellar models. Our analysis was specifically designed to detect the presence of young stellar populations. Therefore, we significantly increased the

frequency of theoretical models contributing to the linear combination for ages <20 Ma (three models were considered: 5, 10 and 20 Ma). Given that there is no stellar overdensity that would be indicative of the presence of non-dissolved clusters in the Sgr B1 region, we chose the youngest model (5 Ma) in agreement with stars with ages slightly older than the known young clusters Arches and Quintuplet[32,35].

Supplementary Fig. 8 shows a comparison between stellar models in the range of 1–20 Ma to assess whether the chosen models were a good reference for all the possible young ages. We conclude that there was a smooth transition between the different stellar populations and that the 5, 10 and 20 Ma models represent good choices to properly cover this range of ages.

Total mass estimation. We estimated the total stellar mass in the Sgr B1 region using the results obtained by fitting PARSEC models. For this, we scaled the bin width of the KLF to the theoretical models' one and computed the stellar mass for each of the Monte Carlo samples by combining the contributions of all the models in a given fit. The final stellar mass was obtained averaging over the results for each of the Monte Carlo samples, where the associated uncertainty was the standard deviation of the mass distribution. The obtained value referred to the mass of the stellar population initially born.

Region of intense hot dust emission. We carried out a dedicated analysis of the central region of Sgr B1, where the presence of hot dust emission is more intense than in the surrounding area based on a Spitzer 4.5 μm image (Fig. 1). We created a KLF and fitted it following the previously explained procedure. Supplementary Fig. 9 shows the obtained results. We found that the contribution from the youngest stellar population is higher than when considering the whole Sgr B1 region analysed, suggesting an excess of young stars in this region. Moreover, we analysed the contribution of the 5–10 Ma and the 10–20 Ma models to each of the Monte Carlo samples (Fig. 5) from both the whole Sgr B1 region and the region of intense hot dust emission. We found that the contribution from the 5–10 Ma stellar population is significantly higher in the region of intense hot dust emission ($6 \pm 1\%$ versus $2 \pm 2\%$). We also found that the contribution from stars in the age bin between 0.5 and 2 Ga is more important, caused by a more significant contribution from the MIST models (that is significantly higher than that for the PARSEC models) to the final result.

To assess the results, we analysed the variation in the contribution of the youngest stellar bin when considering potential sources of systematic uncertainties, as we did in the 'Model fitting and SFH calculation' section for the whole Sgr B1 region. We concluded that the contribution of the youngest stellar population, and thus the detection of one or several dissolved clusters, is unaffected when different bin widths of the KLF, variations in the faint and bright ends of the KLF, a top-heavy IMF and a different completeness solution were considered. On the other hand, we measured a higher contribution of the youngest stellar bin when considering solar metallicity (~14% of the total stellar mass is due to the youngest stellar population) and 1.5 solar metallicity (~10% of the stellar mass due to the youngest stellar population). Therefore, we concluded that the detection of a significant contribution (≳7% of the stellar mass) of the youngest stellar population is robust.

To assess the age estimate of the youngest stellar population, we repeated our analysis using PARSEC models with ages of 14, 11, 8, 6, 3, 1.5, 0.6, 0.4, 0.2, 0.04, 0.02, 0.01, 0.005 and 0.002 Ga, including a stellar population with an age of 2 Ma to test the influence of a younger stellar population in the modelling. The results are fully compatible within the uncertainties for models assuming the previous stellar ages. We found that the contribution from the 5–10 Ma stellar population is compatible with our results, whereas there is no contribution from the 2 Ma model. In spite of the necessity of spectroscopic follow-up for an accurate age estimation, this indicates that the age that we estimate for the youngest stellar population (5–10 Ma) is consistent and supports a scenario in which the youngest stellar population was not formed in situ.

Tests with artificial SFHs. We assessed the reliability of the KLF fitting method using synthetic SFHs created with PARSEC models assuming twice solar metallicity. We built four different SFHs based on scenarios with and without the presence of young stars (Supplementary Fig. 10). We assumed a stellar mass of $\sim 2.2 \times 10^6\, M_\odot$, similar to that obtained when analysing the region of intense hot dust emission (the region with lowest stellar mass, and thus the most challenging case). We simulated the uncertainties for each stellar bin in agreement with real uncertainties by computing them as the square root of the number of stars in a given magnitude bin. Supplementary Fig. 10a shows the simulated KLFs and how they present different relative contributions of their characteristic features that allow us to reconstruct the SFH via model fitting. We applied the same analysis as for real data and used the same magnitude limits. We found that the method is able to recover all of the simulated SFHs within the 1σ uncertainties (Supplementary Fig. 10b).

Comparison with the Quintuplet cluster. We compared the results obtained for the region of intense hot dust emission with a region of the same size containing the Quintuplet cluster (F10 field of the GALACTICNUCLEUS survey[13], see the 'Data' section). Supplementary Fig. 11 shows the results obtained after applying our KLF fitting technique using PARSEC and MIST models. We observed that the uncertainties are higher than for the Sgr B1 region with intense hot dust emission. This is due to the lower data completeness in this region, which limits the faint end of KLF to $K_s \approx 15$ mag (~1 mag lower than for the Sgr B1 region). We estimated that the contribution of the very young stars considering the 5 + 10 Ma stellar models (the estimated age of the Quintuplet cluster is ~5 Ma) is $1.3 \pm 0.9\%$ of the total stellar mass in the region. This means a young stellar mass of $6.8 \pm 0.5 \times 10^4\, M_\odot$, which is of the same order of magnitude as the estimated mass for the Quintuplet cluster ($\sim 10^4\, M_\odot$), revealing its presence in the analysed region and indicating that the method is capable of identifying young stars in a given field. A more precise measurement of the total young stellar mass would require deeper photometry to better constrain the faint end of the KLF.

Data availability

All the raw data used in this study are available at the ESO Science Archive Facility (http://archive.eso.org/eso/eso_archive_main.html) under programme ID 195.B-0283 (https://archive.eso.org/scienceportal/home?data_collection=195.B-0283). The final version of the GALACTICNUCLEUS survey (images and point source catalogues) is publicly available via the ESO phase 3 data release interface (https://www.eso.org/qi/catalogQuery/index/369).

Code availability

The analysis of the luminosity function was performed using the Python SciPy version 1.2.1 package (https://scipy.org). The Parsec[21–23] and MIST[24–26] models used are publicly available at http://stev.oapd.inaf.it/cgi-bin/cmd and https://waps.cfa.harvard.edu/MIST/, respectively. The main codes used for the analysis are publicly available at https://github.com/fnogueras/Codes_GC_young_stars_excess. Other scripts corresponding to particular steps of the analysis can be obtained from the corresponding author upon reasonable request.

Received: 15 February 2022; Accepted: 5 July 2022;
Published online: 25 August 2022

References

1. Nogueras-Lara, F. et al. GALACTICNUCLEUS: a high angular resolution JHKs imaging survey of the Galactic centre. I. Methodology, performance, and near-infrared extinction towards the Galactic centre. *Astron. Astrophys.* **610**, A83 (2018).
2. Nogueras-Lara, F. et al. GALACTICNUCLEUS: a high angular resolution JHKs imaging survey of the Galactic centre. II. First data release of the catalogue and the most detailed CMDs of the GC. *Astron. Astrophys.* **631**, A20 (2019).
3. Launhardt, R., Zylka, R. & Mezger, P. G. The nuclear bulge of the Galaxy. III. Large-scale physical characteristics of stars and interstellar matter. *Astron. Astrophys.* **384**, 112–139 (2002).
4. Nogueras-Lara, F. et al. Early formation and recent starburst activity in the nuclear disk of the Milky Way. *Nat. Astron.* **4**, 377–381 (2020).
5. Nishiyama, S. et al. The interstellar extinction law toward the Galactic Center. II Y, J, H, and Ks Bands. *Astrophys. J.* **680**, 1174–1179 (2008).
6. Morris, M. & Serabyn, E. The galactic center environment. *Annu. Rev. Astron. Astrophys.* **34**, 645–701 (1996).
7. Mezger, P.-G., Duschl, W.-J. & Zylka, R. The Galactic Center: a laboratory for AGN? *Astron. Astrophys. Rev.* **7**, 289–388 (1996).
8. Matsunaga, N. et al. Three classical Cepheid variable stars in the nuclear bulge of the Milky Way. *Nature* **477**, 188–190 (2011).
9. Barnes, A. T. et al. Star formation rates and efficiencies in the Galactic Centre. *Mon. Not. R. Astron. Soc.* **469**, 2263–2285 (2017).
10. Crocker, R. M. et al. Wild at heart: the particle astrophysics of the Galactic Centre. *Mon. Not. R. Astron. Soc.* **431**, 763–788 (2011).
11. Mauerhan, J. C., Muno, M. P., Morris, M. R., Stolovy, S. R. & Cotera, A. Near-infrared counterparts to Chandra X-ray sources toward the Galactic Center. II. Discovery of Wolf-Rayet stars and O supergiants. *Astrophys. J.* **710**, 706 (2010).
12. Schneider, F. R. N. et al. Ages of young star clusters, massive blue stragglers, and the upper mass limit of stars: analyzing age-dependent stellar mass functions. *Astrophys. J.* **780**, 117 (2014).
13. Portegies-Zwart, S. F., Makino, J., McMillan, S. L. W. & Hut, P. The lives and deaths of star clusters near the galactic center. *Astrophys. J.* **565**, 265–279 (2002).
14. Kruijssen, J. M. D. et al. What controls star formation in the central 500 pc of the Galaxy? *Mon. Not. R. Astron. Soc.* **440**, 3370–3391 (2014).
15. Nogueras-Lara, F., Schödel, R. & Neumayer, N. GALACTICNUCLEUS: a high-angular-resolution JHKs imaging survey of the Galactic centre. IV. Extinction maps and de-reddened photometry. *Astron. Astrophys.* **653**, A133 (2021).
16. Simpson, J. P., Colgan, S. W. J., Cotera, A. S., Kaufman, M. J. & Stolovy, S. R. SOFIA FIFI-LS observations of Sgr B1: ionization structure and sources of excitation. *Astrophys. J. Lett.* **867**, L13 (2018).
17. Simpson, J. P., Colgan, S. W. J., Cotera, A. S., Kaufman, M. J. & Stolovy, S. R. Sagittarius B1: a patchwork of H II regions and photodissociation regions. *Astrophys. J.* **910**, 59 (2021).

18. Clark, J. S., Patrick, L. R., Najarro, F., Evans, C. J. & Lohr, M. Constraining the population of isolated massive stars within the central molecular zone. *Astron. Astrophys.* **649**, A43 (2021).
19. Nogueras-Lara, F., Schödel, R. & Neumayer, N. Distance and extinction to the Milky Way spiral arms along the Galactic centre line of sight. *Astron. Astrophys.* **653**, A33 (2021).
20. Schödel, R. et al. The Milky Way's nuclear star cluster: old, metal-rich, and cuspy. Structure and star formation history from deep imaging. *Astron. Astrophys.* **641**, A102 (2020).
21. Bressan, A. et al. PARSEC: stellar tracks and isochrones with the PAdova and TRieste Stellar Evolution Code. *Mon. Not. R. Astron. Soc.* **427**, 127–145 (2012).
22. Chen, Y. et al. Improving PARSEC models for very low mass stars. *Mon. Not. R. Astron. Soc.* **444**, 2525–2543 (2014).
23. Chen, Y. et al. PARSEC evolutionary tracks of massive stars up to 350 $M_{\odot}$ at metallicities $0.0001<Z<0.04$. *Mon. Not. R. Astron. Soc.* **452**, 1068–1080 (2015).
24. Dotter, A. MESA Isochrones and Stellar Tracks (MIST) 0: methods for the construction of stellar isochrones. *Astrophys. J. Suppl. Ser.* **222**, 8 (2016).
25. Choi, J. et al. Mesa Isochrones and Stellar Tracks (MIST). I. Solar-scaled models. *Astrophys. J.* **823**, 102 (2016).
26. Paxton, B. et al. Modules for Experiments in Stellar Astrophysics (MESA). *Astrophys. J. Suppl. Ser.* **192**, 3 (2011).
27. Schultheis, M. et al. The inner two degrees of the Milky Way. Evidence of a chemical difference between the Galactic Center and the surrounding inner bulge stellar populations. *Astron. Astrophys.* **627**, A152 (2019).
28. Schultheis, M. et al. The nuclear stellar disc of the Milky Way: a dynamically cool and metal-rich component possibly formed from the central molecular zone. *Astron. Astrophys.* **650**, A191 (2021).
29. Nogueras-Lara, F., Schödel, R. & Neumayer, N. The nuclear star cluster and nuclear stellar disk of the Milky Way: different stellar populations and star formation histories. *Astrophys. J.* **920**, 97 (2021).
30. Shahzamanian, B. et al. First results from a large-scale proper motion study of the Galactic centre. *Astron. Astrophys.* **632**, A116 (2019).
31. Bittner, A. et al. Inside-out formation of nuclear discs and the absence of old central spheroids in barred galaxies of the TIMER survey. *Astron. Astrophys.* **643**, A65 (2020).
32. Rui, N. Z. et al. The Quintuplet cluster: extended structure and tidal radius. *Astrophys. J.* **877**, 37 (2019).
33. Clarkson, W.-I. et al. Proper motions of the Arches cluster with keck laser guide star adaptive optics: the first kinematic mass measurement of the Arches. *Astrophys. J.* **751**, 132 (2012).
34. Stolovy, S. et al. A mid-infrared survey of the inner 2x1.5 degrees of the Galaxy with Spitzer/IRAC. *J. Phys. Conf. Ser.* **54**, 176–182 (2006).
35. Sormani, M. C. et al. Self-consistent modelling of the Milky Way's nuclear stellar disc. *Mon. Not. R. Astron. Soc.* **512**, 1857–1884 (2022).
36. Simpson, J. P. Spitzer infrared spectrograph observations of the Galactic Center: quantifying the extreme ultraviolet/soft X-ray fluxes. *Astrophys. J.* **857**, 59 (2018).
37. Wang, Q. D., Dong, H. & Lang, C. The interplay between star formation and the nuclear environment of our Galaxy: deep X-ray observations of the Galactic centre Arches and Quintuplet clusters. *Mon. Not. R. Astron. Soc.* **371**, 38–54 (2006).
38. Nobukawa, M. et al. Suzaku spectroscopy of an X-ray reflection nebula and a new supernova remnant candidate in the SgrB1 region. *Publ. Astron. Soc. Pac.* **60**, S191 (2008).
39. Trujillo-Gomez, S., Reina-Campos, M. & Kruijssen, J.-M. Diederik A model for the minimum mass of bound stellar clusters and its dependence on the galactic environment. *Mon. Not. R. Astron. Soc.* **488**, 3972–3994 (2019).
40. Ginsburg, A. & Kruijssen, J.-M. Diederik A high cluster formation efficiency in the Sagittarius B2 complex. *Astrophys. J. Lett.* **864**, L17 (2018).
41. Armillotta, L., Krumholz, M. R., Di Teodoro, E. M. & McClure-Griffiths, N. M. The life cycle of the central molecular zone – I. Inflow, star formation, and winds. *Mon. Not. R. Astron. Soc.* **490**, 4401–4418 (2019).
42. Libralato, M. et al. 2D kinematics of massive stars near the Galactic Centre. *Mon. Not. R. Astron. Soc.* **500**, 3213–3239 (2021).
43. Nishiyama, S. et al. Interstellar extinction law in the J, H, and K_s bands toward the Galactic Center. *Astrophys. J.* **638**, 839–846 (2006).
44. Girardi, L. Red clump stars. *Annu. Rev. Astron. Astrophys.* **54**, 95–133 (2016).
45. Nogueras-Lara, F. et al. GALACTICNUCLEUS: a high-angular-resolution JHKs imaging survey of the Galactic centre. III. Evidence for wavelength-dependence of the extinction curve in the near-infrared. *Astron. Astrophys.* **641**, A141 (2021).
46. Freedman, D. & Diaconis, P. On the histogram as a density estimator: L2 theory. *Probab. Theory Relat. Fields* **57**, 453–476 (1981).
47. Sturges, H. A. The choice of a class interval. *J. Am. Stat. Assoc.* **21**, 65–66 (1926).
48. Diolaiti, E. et al. StarFinder: an IDL GUI-based code to analyze crowded fields with isoplanatic correcting PSF fitting. *Proc. SPIE* **4007**, 879–888 (2000).
49. Matsunaga, N. et al. A near-infrared survey of Miras and the distance to the Galactic Centre. *Mon. Not. R. Astron. Soc.* **399**, 1709–1729 (2009).
50. Skrutskie, M.-F. et al. The Two Micron All Sky Survey (2MASS). *Astron. J.* **131**, 1163 (2006).
51. Alves, D. R. & Sarajedini, A. The age-dependent luminosities of the red giant branch bump, asymptotic giant branch bump, and horizontal branch red clump. *Astrophys. J.* **511**, 225 (1999).
52. Nogueras-Lara, F. et al. Star formation history and metallicity in the Galactic inner bulge revealed by the red giant branch bump. *Astron. Astrophys.* **620**, A83 (2018).
53. Oswalt, T. D. & Gilmore, G. (eds) *Planets, Stars and Stellar Systems*, Vol. 5 (Springer Science+Business Media Dordrecht, 2013).
54. Eisenhauer, F., Quirrenbach, A., Zinnecker, H. & Genzel, R. Stellar content of the galactic starburst template NGC 3603 from adaptive optics observations. *Astrophys. J.* **498**, 278 (1998).
55. Najarro, F., Figer, D.-F., Hillier, D.-J., Geballe, T.-R. & Kudritzki, R.-P. Metallicity in the Galactic Center: the Quintuplet cluster. *Astrophys. J.* **691**, 1816 (2009).
56. Moe, M. & Di Stefano, R. Mind your ps and qs: the interrelation between period (P) and mass-ratio (Q) distributions of binary stars. *Astrophys. J. Suppl. Ser.* **230**, 15 (2017).
57. Hosek, M. W. Jr. et al. SPISEA: a Python-based simple stellar population synthesis code for star clusters. *Astron. J.* **160**, 143 (2020).
58. Lu, J.-R. et al. Stellar populations in the central 0.5 pc of the Galaxy. II. The initial mass function. *Astrophys. J.* **764**, 155 (2013).

Acknowledgements

This work is based on observations made with ESO Telescopes at the La Silla Paranal Observatory under programme ID 195.B-0283. We thank the staff of the ESO for their great efforts and helpfulness. F.N.-L. acknowledges sponsorship provided by the Federal Ministry for Education and Research of Germany through the Alexander von Humboldt Foundation. R.S. acknowledges financial support from the State Agency for Research of the Spanish MCIU through the 'Center of Excellence Severo Ochoa' award for the Instituto de Astrofísica de Andalucía (grant number SEV-2017-0709). R.S. acknowledges financial support from national project PGC2018-095049-B-C21 (MCIU/AEI/FEDER, UE) and financial support from grant number P20-00753 awarded by Junta de Andalucía (Autonomical Government of Andalusia, Spain). N.N. gratefully acknowledges support from the Deutsche Forschungsgemeinschaft (DFG, German Research Foundation) Project-ID 138713538 SFB 881 ('The Milky Way System', subproject B8). F.N.-L. thanks D. Kruijssen, A. Ginsburg and A. Barnes for useful discussions.

Author contributions

F.N.-L. led and carried out the analysis, reduced the data and wrote the manuscript. R.S. is the PI of the GALACTICNUCLEUS project and produced the MIST KLFs. N.N. and R.S. contributed to the interpretation and the discussion of the results and helped organize and edit the final version of the manuscript.

Funding

Open access funding provided by Max Planck Society

Competing interests

The authors declare no competing interests.

Additional information

Supplementary information The online version contains supplementary material available at https://doi.org/10.1038/s41550-022-01755-3.

Correspondence and requests for materials should be addressed to Francisco Nogueras-Lara.

Peer review information *Nature Astronomy* thanks Lee Patrick and the other, anonymous, reviewer(s) for their contribution to the peer review of this work.